

Section 9

Development of and studies with coupled and Earth system models and data assimilation systems.

Natural CO₂ fluxes in Russia in the 21st century and their contribution to climate change: Multimodel estimates

Sergey N Denisov, Igor I Mokhov

*A.M. Obukhov Institute of Atmospheric Physics, RAS, Moscow, Russia
denisov@ifaran.ru*

Russia's carbon balance plays an important role in the global carbon cycle due to large areas of forests, peatlands and wetlands and significant soil carbon pool. Most of Russia's territory is located in the permafrost zone. In these areas over thousands of years, large reserves of carbon have formed in lake sediments and in marsh, forest and tundra soils. As a result of climatic changes, the balance between carbon inflow to soil reservoirs and its emission in the form of CO₂ may change greatly due to increased heterotrophic respiration of the soil.

In [1], estimates of changes in natural CO₂ fluxes in Russia in the 21st century and their possible contribution to climate change were obtained using the Earth System Model of the A.M. Obukhov Institute of Atmospheric Physics RAS (IAP RAS ESM). It was shown that the uptake of CO₂ by terrestrial ecosystems in Russia under all the scenarios of anthropogenic impact considered reaches a maximum by the middle of the 21st century and then decreases. Carbon dioxide fluxes have a high variability and their estimates according to different models differ greatly even for the modern period. Therefore, it is important to estimate the possible range of changes in greenhouse gas fluxes and their contribution to climate change on a larger data set. To investigate the range of CO₂ flux estimates, data from Earth System Models of the CMIP6 project for the 21st century under various scenarios of anthropogenic forcings were used (see also [2]).

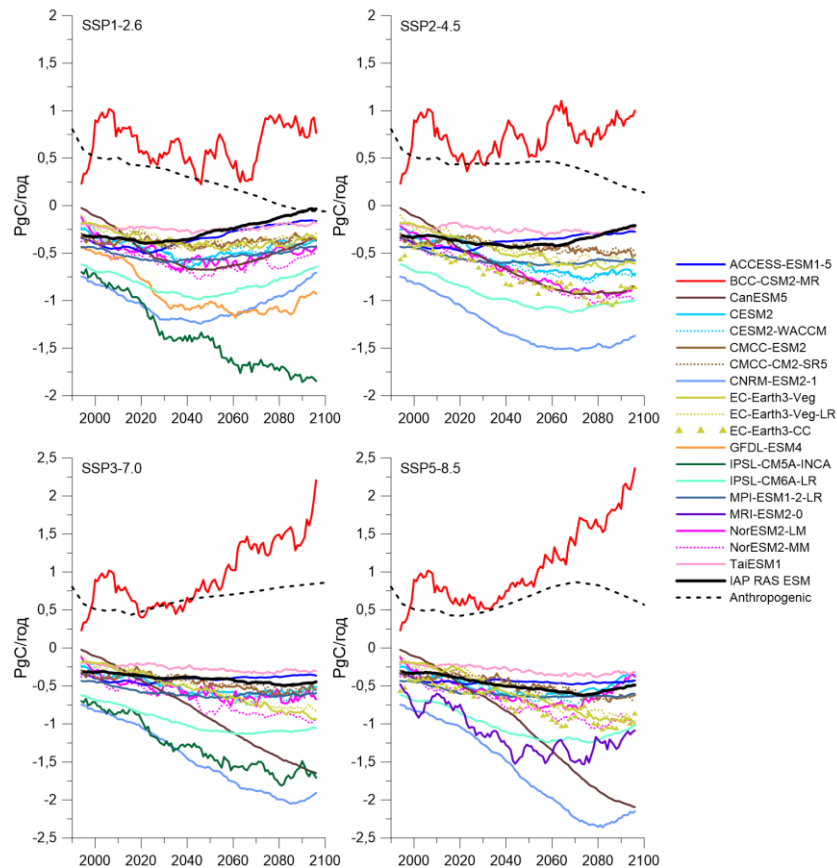


Figure 1. Natural CO₂ fluxes into the atmosphere from the terrestrial territory of Russia under different scenarios of anthropogenic impact on the climate.

Fig. 1 shows the total natural annual fluxes of CO₂ from terrestrial ecosystems into the atmosphere on the territory of Russia (the so-called net ecosystem production, NEP). The negative values correspond to

the absorption of CO₂ from the atmosphere. Due to the high variability of the fluxes, all data are presented with a 9-year moving averaging.

In the 21st century, the discrepancy in flux estimates between models is growing. The largest range of estimates from -2.5 to 2.5 GtC/yr is reached at the end of the 21st century under the scenario with the greatest anthropogenic impact on the climate SSP5-8.5. Anthropogenic CO₂ emissions from the territory of Russia are in the same range as natural fluxes and can be largely compensated by them.

Estimates of CO₂ fluxes using the IAP RAS ESM correspond to the range of CMIP6 estimates throughout the 21st century under all anthropogenic forcing scenarios. The trend towards reduction of carbon dioxide uptake by terrestrial ecosystems by the end of the 21st century obtained for the IAP RAS ESM [1] is also characteristic of many other CMIP6 models.

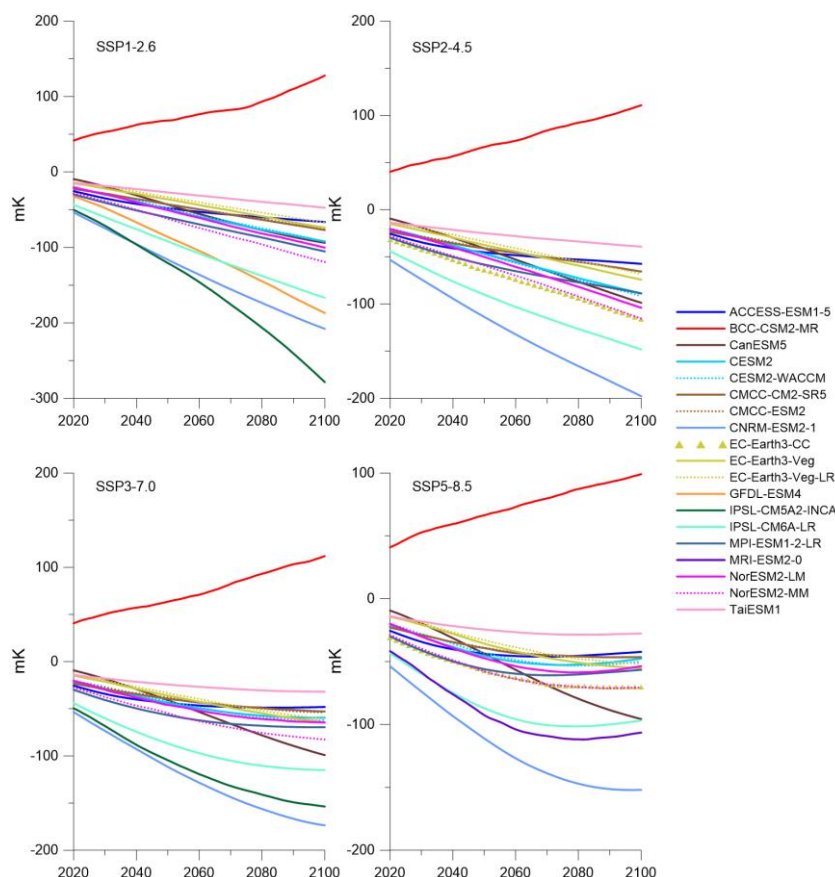


Figure 2. Cumulative temperature potential of natural CO₂ fluxes [mK] in the territory of Russia since 1990 under different scenarios of anthropogenic impact on the climate.

The cumulative temperature potential of natural CO₂ fluxes in Russia from 1990 to the end of the 21st century according to estimates based on data from CMIP6 models equals, depending on the scenario of anthropogenic impact, from -0.3 to 0.1 K (Fig. 2). As in the case of CO₂ fluxes, the range of estimates is reduced if the main group of models is distinguished. The trend noted earlier for the IAP RAS ESM of slowing growth and even weakening of the stabilizing contribution of terrestrial ecosystems of Russia to global climate change [1] can also be noted for many of the CMIP6 models, especially under scenarios with strong anthropogenic forcings.

This work was supported by the Russian Science Foundation (project 19-17-00240).

1. Denisov S.N., Eliseev A.V., Mokhov I.I. Contribution of natural and anthropogenic emissions of CO₂ and CH₄ to the atmosphere from the territory of Russia to global climate change in the 21st century. *Doklady Earth Sciences*, 2019, **488**(1), 1066–1071.

2. Denisov S.N., Mokhov I.I. Estimates of contemporary natural carbon dioxide fluxes in Russia and their uncertainties based on CMIP6 ensemble data. *Research Activities in Earth System Modelling*. E. Astakhova (ed.), 2022, WCRP Rep. No. 4/2022, S. 7, 5-6.

Domain expansion and nudging method of JMA's Local Chemical Transport Model

KAMADA Akane¹, YAMAGUCHI Haruki¹, KAJINO Mizuo²

¹Numerical Prediction Development Center, Japan Meteorological Agency

²Meteorological Research Institute, Japan Meteorological Agency

E-mail: a.kamada@met.kishou.go.jp

1. Introduction

JMA introduced a regional Chemical Transport Model (NHM-Chem; Kajino et al. 2019; 20-km resolution) to support air quality forecasting for smog information in March 2015, and added a local CTM (ASUCA-Chem; Kajino et al. 2022; 5-km resolution) for more detailed forecasting in March 2021 with assimilation of in-situ surface ozone observation data starting in June 2022. The calculation domain of the local CTM was also expanded in February 2023 for effective issuance of operational smog information (Figure 1), and its ozone boundary conditions were changed to JMA's global CTM from the regional CTM. The model after domain expansion is referred to as the local CTM here to distinguish it from the regional CTM. The local domains differ.

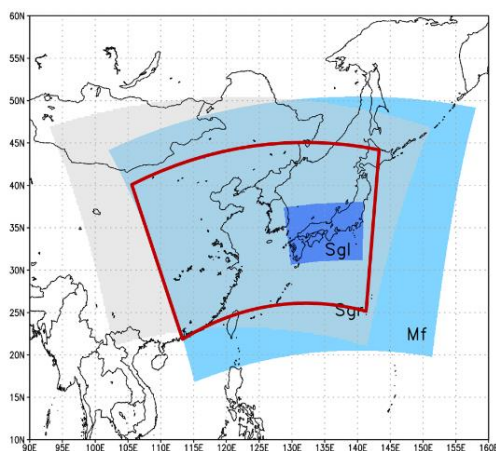


Figure.1 Calculation domains for JMA's MSM (light blue), regional CTM (grey), previous CTM (blue) and new local CTM (red)

2. Model and data assimilation

Output from the JMA Meso-Scale Model (MSM) is used for local CTM meteorological fields, and simplification is applied in forecasting of surface photochemical oxidants to reduce computational costs. The horizontal resolution is 5×5 km in Lambert coordinates, and the vertical resolution has 19 levels in terrain-following coordinates from the ground surface to 10 km above sea level.

The local CTM operationally runs over 51 hours with an initial time of 12 UTC once a day, assimilating surface ozone concentration data (AEROS: Atmospheric Environmental Regional Observation System in Japan) during the first 6 hours. Nudging is applied for data assimilation as with the regional CTM (JMA 2023).

3. Experiment

Forecasts from the new local CTM with data assimilation and the expanded domain were tested (Sgl-TEST) and compared with operational forecasts from the regional CTM (Sgr-CNTL) and the previous version of the local CTM (Sgl-CNTL). The comparison periods were 1 April – 15 June 2022 and 16 June – 30 September 2022 in consideration of the timing of data assimilation into Sgl-CNTL on 15 June 2022.

Figure 2 shows an event involving high surface ozone concentration when smog information was issued. Sgl-TEST and Sgl-CNTL show quantitatively consistent distribution to AEROS and more precise distribution than Sgr-CNTL.

The root mean square error (RMSE) of Sgl-TEST in spring was generally smaller than those of Sgr-CNTL and Sgl-CNTL (Figure 3), showing the effects of data assimilation for the lead time of 6 hours and until morning during the forecast period. In regard to the high ozone concentration that often occurs in coastal metropolitan areas and then moves inland during daytime in summer, Sgl-TEST and Sgl-CNTL tended to overestimate surface ozone concentration in inland areas, and related RMSEs were generally higher than those of Sgr-CNTL. Sgl-TEST forecasted surface ozone better than Sgr-CNTL for nighttime periods and in coastal areas (not shown).

4. Summary

JMA originally had two CTMs with different resolutions

and domains for photochemical smog bulletins. New data assimilation and domain expansion for the higher-resolution CTM optimized forecast skill for surface ozone concentration. As a result, the lower-resolution CTM was replaced with the higher-resolution version in February 2023.

References

JMA, 2023: Outline of the operational numerical weather prediction at the Japan Meteorological Agency. Appendix to WMO Technical Progress Report on the Global Data-processing and Forecasting System and Numerical Weather Prediction, Japan Meteorological Agency, Tokyo, Japan.

Kajino, M., M. Deushi, T. T. Sekiyama, N. Oshima, K. Yumimoto, T. Y. Tanaka, J. Ching, A. Hashimoto, T.

Yamamoto, M. Ikegami, A. Kamada, M. Miyashita, Y. Inomata, S. Shima, A. Takami, A. Shimizu, S. Hatakeyama, Y. Sadanaga, H. Irie, K. Adachi, Y. Zaizen, Y. Igarashi, H. Ueda, T. Maki, and M. Mikami, 2019: NHM-Chem, the Japan Meteorological Agency’s Regional Meteorology – Chemistry Model: Model Evaluations toward the Consistent Predictions of the Chemical, Physical, and Optical Properties of Aerosols. *J. Meteor. Soc. Japan*, 97, 337–374, doi:10.2151/jmsj.2019-020.

Kajino, M., A. Kamada, N. Tanji, M. Kuramochi, M. Deushi, T. Maki, 2022: Quantitative influences of interannual variations in meteorological factors on surface ozone concentration in the hot summer of 2018 in Japan. *Atmos. Environ.: X*, 16, 100191, doi:10.1016/j.aeaoa.2022.100191.

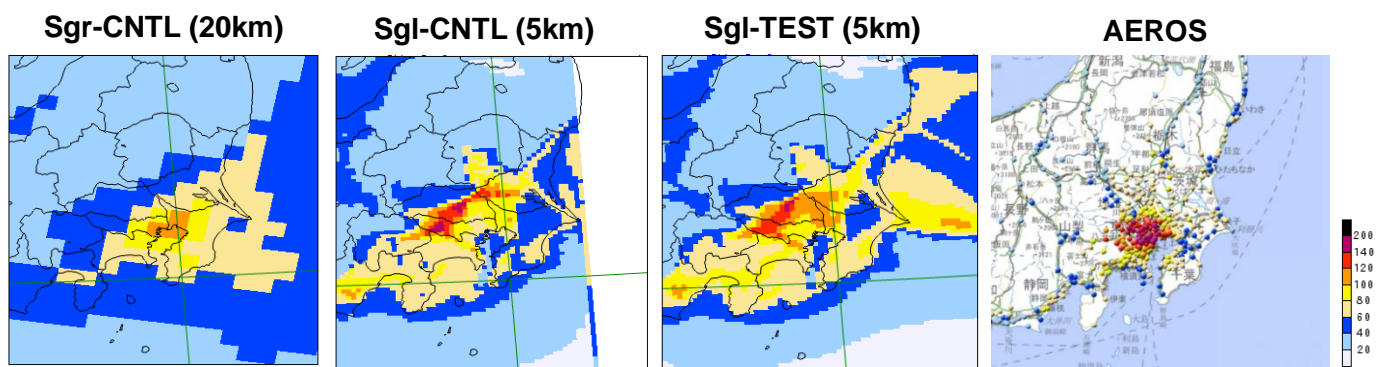


Figure.2 Surface ozone concentration at 15:00 JST (lead time: 18 hrs) on June 30 2022. AEROS data are mapped under GSI Tiles at <https://maps.gsi.go.jp/development/ichiran.html>.

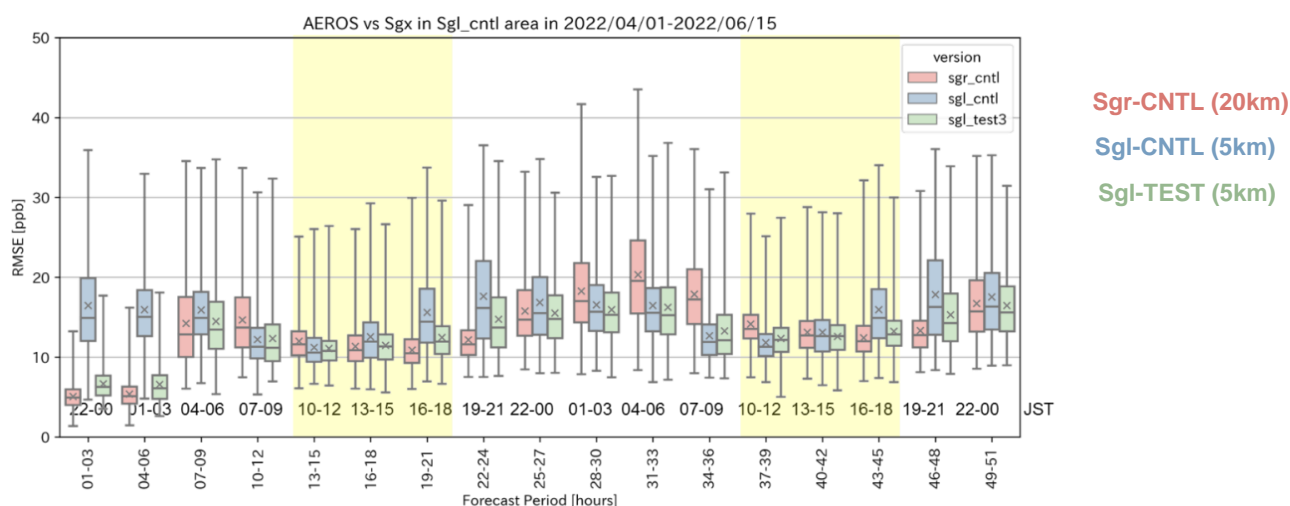


Figure.3 RMSEs of spring surface ozone forecasts from Sgr-CNTL (red), Sgl-CNTL (blue) and Sgl-TEST (green). Horizontal axis: lead time; yellow shading: daytime hours; whiskers: 0th and 100th percentile; boxes 25th – 75th percentiles; bars: 50th percentile; x: mean

Implementation of subseasonal drought monitoring from NCMRWF Extended Range Prediction System

Kondapalli Niranjan Kumar, Ankur Gupta, Imranali M Momin, A K Mishra, R Ashrit, A K Mitra & V S Prasad

National Centre for Medium Range Weather Forecasting, Ministry of Earth Sciences, Noida, India

Email: niranjan.kondapalli@gov.in

1. Background

Drought is a natural phenomenon characterized by an extended period of abnormally dry weather conditions, resulting in a significant water shortage. Consequently, drought poses a significant threat to water resources, including surface water and groundwater reserves resulting in a deficit water supply for irrigation, drinking water, and industrial use with heavy consequences for the local population. Hence, drought planning and management is essential to developing early warning systems, and drought response strategies that can enhance resilience and aid in proactive decision-making. The countries like India where the livelihood of 60% of the population depends on agriculture, drought is one of the most feared natural calamities as it impacts food production, economy, and morale of millions of farmers in the country. More importantly, recent studies stressed on flash droughts are characterized by rapid onset and intensification, unfolding on sub-seasonal to seasonal (S2S) time scales. To monitor and assess drought conditions, various tools and indices are used, including the Standardized Precipitation Index (SPI), Palmer Drought Severity Index (PDSI) etc. The SPI was designed to quantify the rainfall deficit to monitor drought conditions on a range of time scales. This temporal flexibility allows SPI to be useful in short-term agricultural and long-term hydrological applications. Therefore, we strategically started the drought monitoring system using the SPI estimated based on National Centre for Medium Range Weather Forecasting (NCMRWF) Extended Range Prediction (NERP) System. The following section discusses briefly the NERP modelling system.

2. NCMRWF Extended Range Prediction System

The NERP model configuration is based on the UK Met Office GloSea5 seasonal prediction system in Global Coupled 2.0 configuration (GC2.0; documented in Williams et al., 2015). The model is a fully global coupled S2S ensemble system consisting of Global Atmosphere 6.0 (GA6.0) and Global Land 6.0 (GL6.0), GlobalOcean 5.0 (GO5.0) and Global Sea Ice 6.0 (GSI6.0) (Walters et al., 2017; Gupta et al., 2019 and references therein). The atmospheric model is non-hydrostatic and fully compressible with semi-implicit semi-Lagrangian discretization to solve equations of motion. The model has a terrain-following hybrid-height coordinate system with a horizontal resolution of $0.833^\circ \times 0.556^\circ$ having 85 vertical levels covering up to 85 km. The NERP operational model has 16 ensemble members obtained from the lagged initial conditions of 4 consecutive preceding days with 4 physically perturbed members generated for each day. The first lagged daily initial condition begins every Sunday and continues until Wednesday every week (Figure 1). The model is integrated into a forecast length of 36 days.

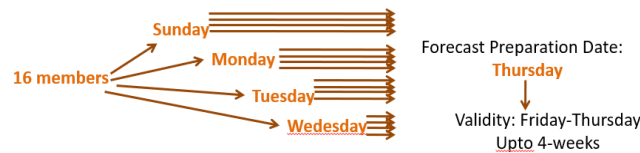


Figure 1 Schematic representing the forecast generation from NERP operational model

3. Multiscalar SPI Drought Outlook

The SPI is calculated by fitting a gamma distribution to the historical precipitation record at each grid location, which is then transformed into a normal distribution so that the mean SPI for the location and desired period is zero (McKee et al., 1993). The positive SPI and negative values represent wet and dry conditions, respectively. The 16-member ensemble mean rainfall is used for computing the SPI drought on weekly/multi-weekly scales. A sample chart of the multi-scalar SPI drought chart released on May 04, 2023, is shown in Figure 2. The drought severity is labelled based on the classification defined by the World Meteorological Organization (WMO). The drought chart indicates the spatiotemporal evolution of drought on weekly scales to multi-week scales that are updated every Friday on www.ncmrwf.gov.in -> Products ->Drought.

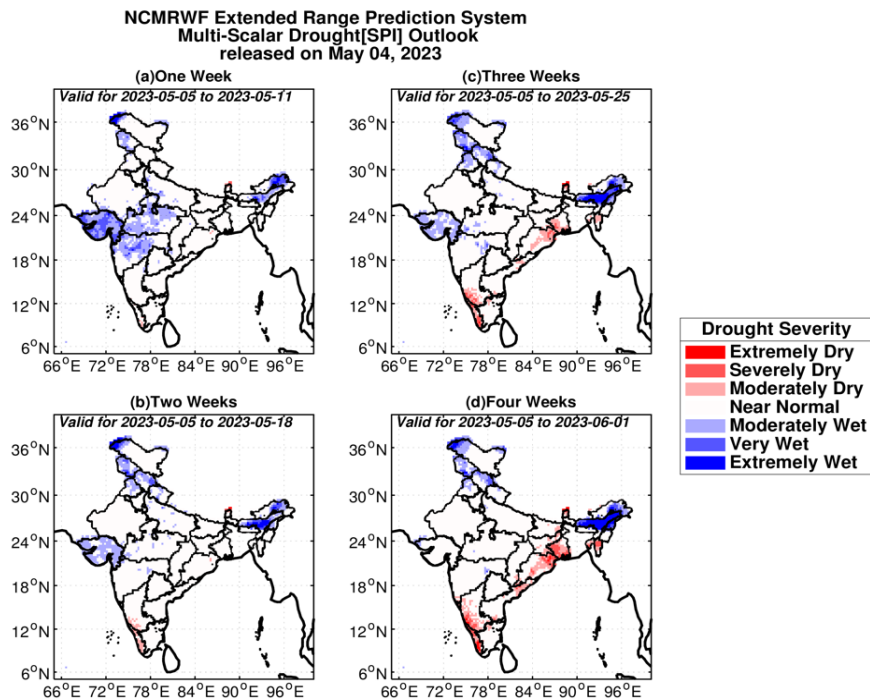


Figure 2 Multi-scalar SPI drought index computed using the NCMRWF extended range prediction system. The climatological distribution is obtained from the India Meteorological Department (IMD) gridded data

4. References

- [1]. Williams, K. D., Harris, C. M., Bodas-Salcedo, A., Camp, J., Comer, R. E., et al. (2015), The Met Office Global Coupled model 2.0 (GC2) configuration, *Geosci. Model Dev.*, 8, 1509–1524, <https://doi.org/10.5194/gmd-8-1509-2015>
- [2]. Walters, D., Boutle, I., Brooks, M., et al. (2017), The Met Office Unified Model Global Atmosphere 6.0/6.1 and JULES Global Land 6.0/6.1 configurations, *Geosci. Model Dev.*, 10, 1487–1520, <https://doi.org/10.5194/gmd-10-1487-2017>
- [3]. Gupta, A., Ashis K Mitra and E.N. Rajagopal (2019), Implementation of Unified Model based Global Coupled Modelling System at NCMRWF, Technical Report No. NCMRWF/TR/01/2019, https://www.ncmrwf.gov.in/Reports-eng/NCMRWF_Tech_Report_1_2019_CM.pdf

Coupled global Numerical Weather Prediction System at NCMRWF (India) for medium range weather forecast.

Sumit Kumar, Imranali M. Momin and John P. George

National Centre for Medium Range Weather Forecasting (NCMRWF), Ministry of Earth Sciences
(MoES), A-50, Sector-62, Noida UP-201309, India
E-mail address: sumit@ncmrwf.gov.in

National Centre for Medium Range Weather Forecasting (NCMRWF, Ministry of Earth Sciences, Government of India) is an operational numerical weather prediction centre. NCUM global and regional NWP system of NCMRWF has been adapted from Unified Model (UM) seamless prediction system of “UM Partnership”. The NCUM global system, operational since 2012, has been upgraded many times by adapting the improvements in the UM system and through in-house research and development (Sumit et al., 2020). These improvements resulted in significant benefits to the NCUM forecast skill (Sushant et al., 2022). Many improvements were also made to the observation pre-processing system, observation monitoring system, postprocessing of the model forecast etc.

Improving the skill of weather forecast is a continuous process and extend the skilful forecasts to longer lead time is another challenging task. There exists demonstrated evidence that air-sea coupling plays an important role in increasing the forecast skill in the atmosphere at short to extended range (Vellinga et al. 2020). In the uncoupled operational NWP forecasts, SST and sea ice have been prescribed initially to fix the lower boundary conditions for the atmospheric model forecast. However, in the coupled system, atmosphere drives the ocean through the input of momentum, heat, and moisture fluxes whereas the ocean controls the atmosphere through its supplies of moisture and heat. So, in the coupled NWP system, interacting models helped to advance the weather forecast skill through a more physically consistent representation of air-sea interaction.

Table 1: Various Components of Coupled Global assimilation-forecast System (C-NCUM)

Model	Data Assimilation- Atmosphere	Data Assimilation – Land Surface	Data Assimilation- Ocean & Sea Ice
Model: Unified Model; Version 11.9 Domain: Global Horizontal Resolution: 10 km Vertical levels: 70 levels (model top at 80 km) Time step: 4 min.	Method: Incremental 4D-Var Observations assimilated: Observations received at NCMRWF from GTS and other sources. (NOAA/NESDIS, EUMETSAT, ISRO etc.)	Soil Moisture analysis: <i>Method:</i> Simplified Extended Kalman Filter Observations assimilated: ASCAT soil wetness observations, Screen Temperature and Humidity increments (pseudo observations from 3D-Var screen analysis).	Model: NEMO ocean model (Vn 3.6) Resolution: ¼° quasiisotropic resolution (ORCA025 tripolar horizontal grid) Vertical Levels: 75 levels in the vertical varying in thickness. Time step: Both the ocean and CICE model components use a 20min time step. Assimilation method: 3D-Var FGAT (NEMOVAR)
In coupled simulations the atmosphere and land components exchange information with the ocean and sea ice components via the OASIS3 coupler using an hourly coupling frequency			

Implementation of coupled NWP system of “UM Partnership” (Vellinga et al. 2020) at NCMRWF is a major milestone in its progress. This article presents a brief description of the new-coupled NWP system implemented at NCMRWF (C-NCUM). Experimental forecasts run of C-NCUM are being conducted at the NCMRWF Mihir HPC system. The C-NCUM differs in many ways compared to its parent UM coupled system, including very different observation preprocessing. C-NCUM uses an in-house developed atmosphere, ocean, sea ice, land observation preprocessing systems, which uses

observations received at NCMRWF through GTS and various other sources. The data pre-processing system pack the observations in desired format for its further processing, including quality control. The quality-controlled observations are used in the weakly coupled Data Assimilation (DA) system. In the coupled DA system, atmospheric assimilation is based on 4D-Var/Hybrid 4D-Var method, whereas ocean and sea ices assimilation uses 3D-Var and land data assimilation is based on Extended Kalman Filter (EKF) method. Details of the C-NCUM assimilation-forecast system are given in Table-1. There are some differences in observations usage in C-NCUM compared to its parent UM system, like the use of INSAT satellite observations, GeoOptics GPSRO data etc. List of observations assimilated in the coupled C-NCUM is given in Table-2.

Table 2. Observations used for Atmosphere, Land and Ocean assimilation in C-NCUM

Conventional Observations						
Atmosphere: Surface observations over land (SYNOP), SHIP, BUOY (Moored & Drifter), Pilot balloon, Radio-sonde, Wind Profiler, DWR, VAD Winds, Aircraft observations, GroundGPS						
Ocean: Temperature and salinity profile (XBT-TESAC), ARGO, BUOY (Moored & Drifter)						
Satellite Observations						
	Radiances		Satellite AMVs		Scatterometer Winds	GPSRO
	Geostationary	Polar	Geostationary	Polar		
Atmosphere	INSAT-3D (Imager & Sounder) SEVIRI (Meteosat-8/10/11), ABI (GOES-16) AHI (HIMAWARI 8/9)	AMSU-A & B (METOPB/C, NOAA-15/18/19) ATMS (SNPP & NOAA20), IASI (METOP B/C), AIRS(AQUA), CrIS (SNPP, NOAA-20) SSMIS (F17), AMSR2 (GCOMW1), GMI-GPM (Low & High),	INSAT3D/3DR, Meteosat-8/10/11/70, HIMAWARI 8 & 9, GOES-16,17,18	NOAA 15/18/19/20, METOP A/B/C MODIS (Aqua & Terra), NPP_Soumi_VIRS	ASCAT (Metop B/C)	COSMIC-2E1-E6, SPIRE, FY-3C/3D, TerraSAR-X, TenDEM, PAZ KOMPSAT-5, METOP-B/C, GeoOptics, GRACE C & D,
Ocean	SST (GHR SST), Sea Level Anomaly (SLA): Sentinel3A/3B/Altika, Sea-Ice Concentration (SSMIS)					
Land	ASCAT soil moisture observations					

Experiments have been carried out with the coupled global NWP system to assess its benefits and limitations, especially over the Indian monsoon region. The results of the studies are encouraging, but more long period studies are needed for robust conclusions. Operational use of the coupled system is planned from last quarter of this year, if the study results support.

References

- Sushant Kumar, Anumeha Dube, Sumit Kumar, S Indira Rani, Kuldeep Sharma, S Karunasagar, Saji Mohandas, Raghavendra Ashrit, John P George & Ashis K Mitra (2022). Improved skill of NCMRWF Unified Model (NCUM-G) in forecasting tropical cyclones over NIO during 2015–2019, *J Earth Syst Sci* 131, 114.
- Sumit Kumar, M. T. Bushair, Buddhi Prakash J., Abhishek Lodh, Priti Sharma, Gibies George, S. Indira Rani, John P. George, A. Jayakumar, Saji Mohandas, Sushant Kumar, Mohana S. Thota, Raghavendra Ashrit, and E. N. Rajagopal (2020). NCUM Global NWP System: Version 6 (NCUM-G:V6), *NCMRWF Technical Report*, NMRF/TR/06/2020
- Vellinga, M., Copesey, D., Graham, T., Milton, S., & Johns, T. (2020). Evaluating Benefits of Two-Way Ocean–Atmosphere Coupling for Global NWP Forecasts, *Weather and Forecast*, 35(5), 2127-2144

Activities of Marchuk Institute of Numerical Mathematics (INM RAS) in climate modelling

E. Volodin

Marchuk Institute of Numerical Mathematics, Moscow, Russia

A coupled atmospheric and oceanic general circulation model (INMCM) has been developed at the Institute of Numerical Mathematics Russian Academy of Sciences (INM RAS). Below is a summary of the recent research with current versions of the model.

1. Climate model versions INMCM48 and INMCM50 have equilibrium climate sensitivity (ECS) about 1.8-1.9 K that is the lowest value among all CMIP6 models (1.8-5.6 K). Now new model versions are developed (Volodin 2023) with ECS about 3.7 K that is twice higher than the earlier value and not far from CMIP6 average. The reasons of low sensitivity in previous versions and increase of ECS in the last version are studied in (Volodin 2021). In general, the new model version reproduces the present-day climate with similar quality or better than the previous version. Figure 1 shows a simulation of global mean surface temperature in an ensemble of historical runs with the new model version.

2. A seasonal forecast system has been developed on the basis of the climate model INMCM50. Verification of seasonal hindcasts shows the quality comparable with other present-day seasonal forecast systems. Figure 2 shows the anomaly correlation coefficient (ACC) for simulation of near surface temperature in DJF of 1993-2009. The global mean ACC for INMCM50 is 0.48, while ACC for a multimodel ensemble presented at <http://wmo.org> is 0.52. Operative seasonal forecasts for 4-10 months with INMCM50 start in test regime each calendar month. The seasonal forecast system on the basis of the INM climate model is described in (Vorobyeva and Volodin 2021).

3. Decadal hindcasts with INMCM50 model were started from each year of 1960-2022. Evaluation of hindcasts shows that the accuracy of climate simulation is comparable with other participants of Annual-to-Decadal Climate Predictions (ADCP). Fig.3 shows ACC for 5-year mean near-surface temperature in INMCM50 hindcasts. The global mean ACC is 0.64. The global mean for other ADCP models presented at (<https://hadleyserver.metoffice.gov.uk/wmolc/> -> Verification, Correlation, Year 1-5: Annual, Temperature) is 0.56-0.67.

References:

Volodin, E. (2021). The mechanisms of cloudiness evolution responsible for equilibrium climate sensitivity in climate model INM-CM4-8. *Geophysical Research Letters*, 48, e2021GL096204.

Vorobyeva, V., Volodin, E. (2021) Evaluation of the INM RAS climate model skill in climate indices and stratospheric anomalies on seasonal timescale. *Tellus, Series A: Dynamic Meteorology and Oceanography* 73(1), <http://doi.org/10.1080/16000870.2021.1892435>

Volodin, E.M. Simulation of Present-Day Climate with the INMCM60 Model. *Izv. Atmos. Ocean. Phys.* 59, 16–22 (2023). <https://doi.org/10.1134/S0001433823010139>

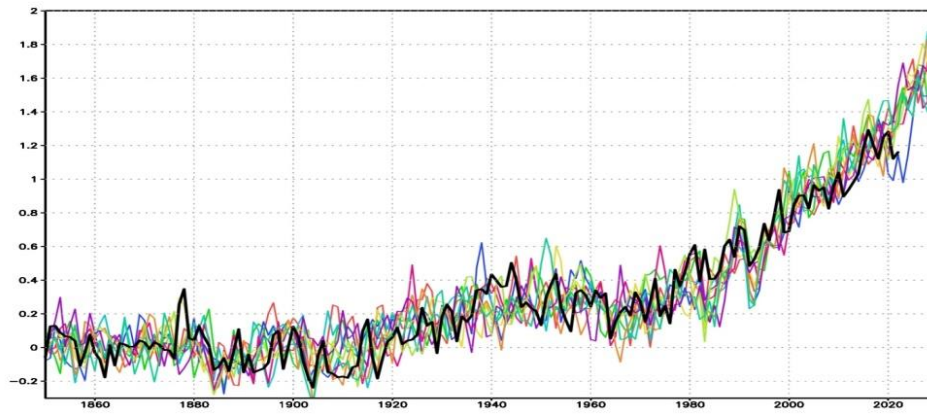


Fig.1. Simulation of global mean surface temperature anomaly with respect to 1850-1899 mean in an ensemble of INM climate model runs (different colors). Observations are shown in bold black line.

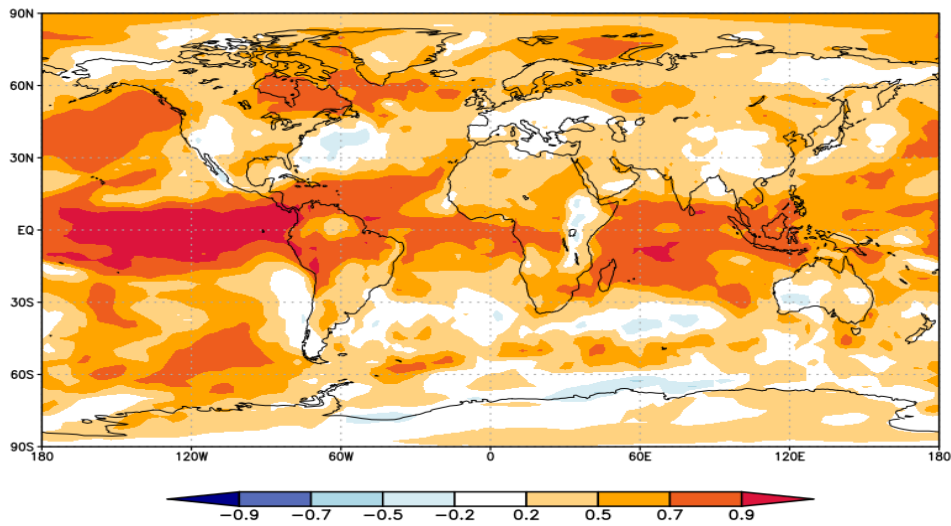


Fig.2. Anomaly correlation coefficient for near surface temperature in seasonal hindcasts with INMCM50 model calculated for DJF of 1993-2009. The global mean is 0.48.

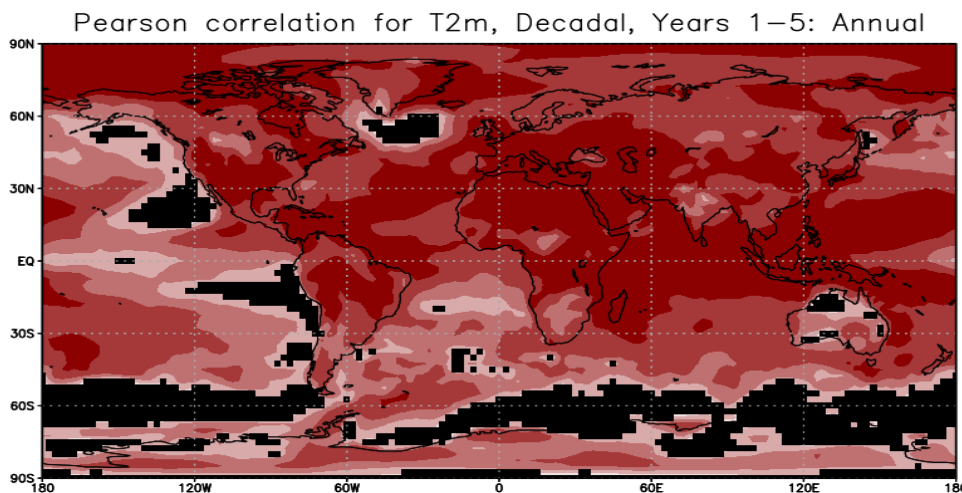


Fig.3. ACC for year 1-5 mean near surface temperature hindcasts for 1960-2017. The global mean value is 0.64.

The impact of ocean coupling on the track simulation of Typhoon Nanmadol (2022)

Akiyoshi Wada

Meteorological Research Institute, Tsukuba, Ibaraki, 305-0052, JAPAN

awada@mri-jma.go.jp

1. Introduction

A tropical depression became Typhoon Nanmadol near the Ogasawara Islands at 18 UTC on 13 September 2022. Nanmadol then rapidly deepened its central pressure from 00 UTC on 15 September, reaching 910 hPa at 18 UTC on 16 September. Although it turned to weaken rapidly north of 28°N from 15 UTC on 17 September, its central pressure was 940 hPa at landfall around Kagoshima. Heavy rainfall was observed around the Kyushu region due to the long duration of developing rain clouds, which may be associated with the track of the typhoon. We conducted numerical simulations on Nanmadol from the early developing phase to the decaying phase using the Japan Meteorological Agency nonhydrostatic atmosphere model (NHM) and the atmosphere-wave-ocean coupled model (CPL: Wada et al., 2018) under different atmospheric conditions at an initial integration time. The simulation results were used to assess the effect of ocean coupling on the track of Nanmadol and the rapid decaying north of 28°N.

2. Experimental design

The following computational domain is the same in all the NHM and CPL experiments. The domain is 4920 km (zonal) x 4740 km (meridional) of which center location is 34.0°N, 140°E. The horizontal resolution is 3 km. The number of vertical layers is 55 (the top height is about 27 km). The time step for the atmosphere model is 10s, that for the ocean model is 60s and that for the ocean surface wave model is 360s. All the simulations are started from 18UTC on 14 September in 2022. The integration period is 105 hours.

An initial condition and 6-hourly boundary conditions for the atmosphere are created from the global objective atmospheric analysis data of the Japan Meteorological Agency (~20 km horizontal resolution). In addition, an initial condition for the ocean is created from the North Pacific version of the oceanic analysis data (~0.1° horizontal resolution) merged with the Optimally Interpolated SST (OISST) daily product (0.25° horizontal resolution) obtained from the Remote Sensing Systems (<http://www.remss.com>) as of 13 September. The Regional Specialized Meteorological Center (RSMC) Tokyo best track data (<https://www.jma.go.jp/jma/jma-eng/jma-center/rsmc-hp-pub-eg/besttrack.html>) is used to validate the results of numerical simulations.

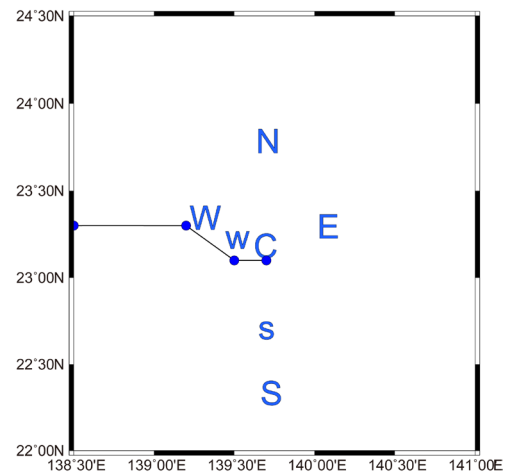


Figure 1 A solid line with closed circles indicates the RSMC-Tokyo best-track locations every 6 hours from 18UTC on 14 to 12 UTC on 15 September. The meaning of alphabets in the panel is explained in the text.

Figure 1 shows the locations of minimum central pressure in each experiment. The character ‘C’ shows the control run. The character ‘N’ means that the atmospheric data at the initial time is shifted northward. The ‘E’, ‘W’ and ‘S’ shows the same meaning as ‘N’ except the direction and distance of the shift. The small characters ‘w’ and ‘s’ are almost the same as ‘W’ and ‘S’ except that the distance of the shift is relatively short. These changes are realized by the modification of Gaussian grid information in the global objective atmospheric analysis data.

3. Results

3.1 Simulated tracks

Figure 2 shows the simulated tracks with the simulated central pressures in all experiments (Fig. 1) simulated by the NHM (Fig. 2a) and CPL (Fig. 2b) with the RSMC-Tokyo best track position with the best-track central pressure. All the simulations tend to show eastward biases after the simulated typhoon passed west of 134°E and north of 26°N compared with the best track. In particular, the eastward biases do increase when the CPL is used instead of the NHM. When shifting the typhoon position south (s or S in Fig. 1) or west (w or W in Fig. 1) at the initial time, the simulated tracks more approach the RSMC best track than that in the other experiments. However, it still fails to simulated the best-track north-westward traveling east of 134°E.

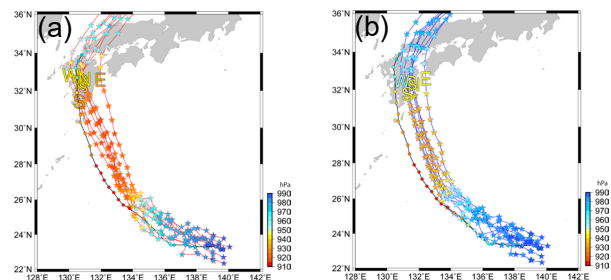


Figure 2 Best track positions every 6 hours with colors indicating the value of best-track central pressures. (a) tracks simulated by the NHM and (b) tracks simulated by the CPL. The alphabets (see Section 2) indicate the location of simulated typhoon at 78 h.

3.2 Simulated central pressures

Figure 3 shows the time series of best track central pressures with individual and ensemble mean central pressures simulated by the NHM and CPL. Central pressures simulated by the NHM tend to be relatively low compared with those simulated by the CPL. The result indicates that ocean coupling helps weaken the intensity of the simulated typhoon irrespective of a different location of the typhoon vortex at the initial time (Fig. 1).

The order of simulated central pressure values among seven numerical experiments at a certain integration time differs between NHM and CPL. The experiment W, which shows the most rapidly deepening and the lowest central pressure in the NHM experiment, does not show such characteristics in the CPL experiment. However, systematic differences in the simulated central pressure between the NHM and CPL experiments may be attributed to the systematic track errors shown in Fig. 2.

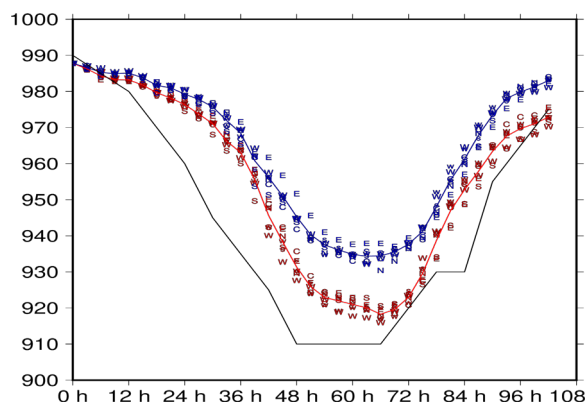


Figure 3 A black solid line indicates the time series of best-track central pressures every 6 hours. Red and blue solid lines indicate the time series of ensemble mean central pressures every 3 hours simulated by the NHM and CPL. The alphabets indicate the result of individual experiment described in Section 2.

3.3 Simulated sea surface temperatures

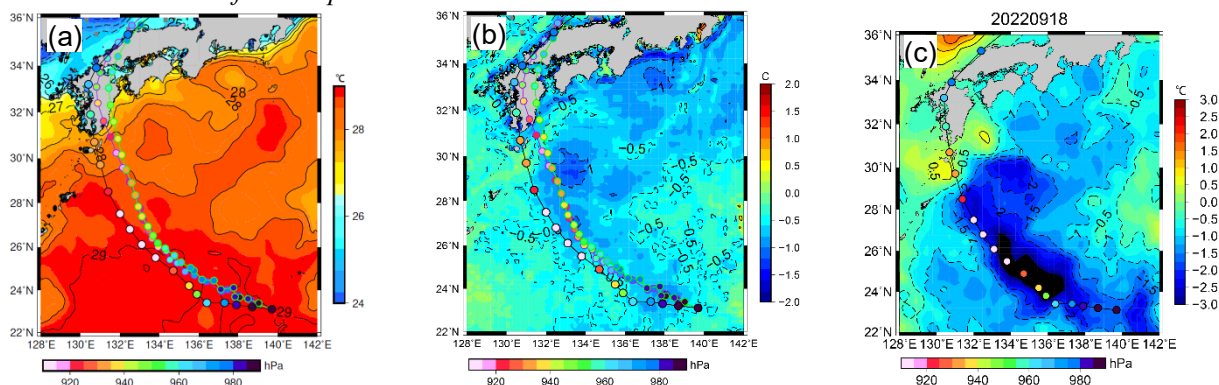


Figure 4 (a) Horizontal distribution of ensemble mean sea surface temperature at 78 h simulated by the CPL with the RSMC best track and tracks by the NHM (purple line) and CPL (green line). (b) Horizontal distribution of the difference in simulated ensemble mean sea surface temperature at 78 h between the NHM and CPL experiments. (c) Horizontal distribution of the variation in microwave optically interpolated sea surface temperature (obtained from <https://www.remss.com/measurements/sea-surface-temperature/>) on 18 September from the sea surface temperature on 13 September. In all panels, colors within the circles indicate the value of central pressure.

Figure 4 shows the horizontal distribution in ensemble mean sea surface temperature at 78 h simulated by the CPL. Sea surface temperature underneath the typhoon does not affect the systematic track errors south of 26°N during the intensification phase since the value of sea surface temperature is higher than 28°C (Fig. 4a) and sea surface cooling along the track is relatively small (Fig. 4b). Simulated decreases in simulated sea surface temperature is remarkable around 29°N , 134°E (Fig. 4b) but decreases in microwave optically interpolated sea surface temperature do appear along the best track even south of 26°N and the magnitude of sea surface cooling is greater than that of simulated sea surface cooling (Fig. 4c). The failure to realistically simulate the minimum sea-level pressure of Nanmadol in the NHM experiments (Fig. 3) may have affected the simulations of track (Fig. 1) and sea surface temperature (Fig. 4a and 4b) in the CPL experiment.

4. Concluding remarks

We show that the simulated track error of Nanmadol may be reduced by changing in the initial position of the typhoon to some extent (within 1 degree) by shifting the atmospheric initial condition. However, it is also clear that this shifting method and ocean coupling does not necessarily improve the systematic track error of Nanmadol west of 134°E . To improve simulated sea surface temperature, realistic simulations on both the intensification rate and the maximum intensity of Nanmadol are required. The improvement of intensity simulations could lead to that of track simulations although the mechanism is not discussed in this report.

It should be noted that the results shown in this study may be different when the other atmosphere-ocean coupled model is used. In addition, the effect of microphysics in the atmosphere model on the track, intensity, and wind rainfall and wind distributions of a typhoon should be explored in the future.

References

Wada, A., S. Kanada, and H. Yamada, 2018: Effect of air–sea environmental conditions and interfacial processes on extremely intense typhoon Haiyan (2013). *Journal of Geophysical Research: Atmospheres*, 123, 10379–10405, <https://doi.org/10.1029/2017JD028139>.

The impact of ocean coupling on the rainfall distribution of Typhoon Nanmadol (2022) at the landfall

Akiyoshi Wada*, Wataru Yanase, and Satoki Tsujino

Meteorological Research Institute, Tsukuba, Ibaraki, 305-0052, JAPAN

*awada@mri-jma.go.jp

1. Introduction

Typhoon Nanmadol (2022) made landfall on Southern Kyushu at 08 UTC on 18 September. The Japan Meteorological Agency (JMA) issued a heavy rain emergency warning for Miyazaki prefecture at around 04 UTC on 14 September before the typhoon made landfall and passed over the region. In fact, the typhoon caused the maximum value on precipitation observations since the start of statistics at several stations in Miyazaki Prefecture (https://www.data.jma.go.jp/miyazaki/shosai/pdf/r4/20220921_saigaiji_houkoku.pdf). To investigate the effect of ocean coupling on the heavy rainfall, we conducted numerical simulations on Nanmadol from the early developing phase to the decaying phase using the JMA nonhydrostatic atmosphere model (NHM), the atmosphere-wave-ocean coupled model (CPL: Wada et al., 2018), the current JMA operational atmosphere model ASUCA, and the ASUCA coupled with a one-dimensional ocean model (OASUCA). The simulation results were used to assess the effect of ocean coupling on the rainfall distribution when the typhoon made landfall on Southern Kyushu.

2. Experimental design

The computational domain is common among the simulations conducted by the NHM and CPL. The domain is 4900 km (zonal) x 4800 km (meridional) of which center location is 30.0°N, 140°E. The horizontal resolution is 2.5 km. The number of vertical layers is 55 for NHM and CPL (the top height is about 27 km). The time step for the atmosphere model is 10 s, that for the ocean model is 60 s and that for the ocean surface wave model is 360 s. The initial time for the simulations by the ASUCA and OASUCA are 00UTC on 15 September in 2022, while that by the NHM and CPL are 18UTC on 14 September in 2022 because the numerical simulations at which initial time is 00 UTC on 15 September has not been complete yet. The integration period is 105 hours.

An initial condition and 6-hourly boundary conditions for the atmosphere are created from the global objective atmospheric analysis data of the Japan Meteorological Agency (~20 km horizontal resolution). The width of lateral boundary relaxation sponge layers is set to be 140 due to the control of track simulations. In addition, an initial condition for the ocean in the NHM and CPL experiments is created from the North Pacific version of the oceanic analysis data (~0.1° horizontal resolution) merged with the Optimally Interpolated SST (OISST) daily product (0.25° horizontal resolution) obtained from the Remote Sensing Systems (<http://www.remss.com>) as of 20 July. In the OASUCA experiment, the World Ocean Atlas (WOA) 2018 (<https://www.ncei.noaa.gov/products/world-ocean-atlas>) and Merged satellite and in-situ data Global Daily Sea Surface Temperature (MGDSST) are used for creating oceanic initial conditions. No boundary condition is used in the CPL experiment, while the simulated sea surface temperature in the OASUCA experiment is restored to the initial condition at a constant time. In the NHM and ASUCA experiments, sea surface temperature is fixed during the integration. Physical processes used in this study are standard as referred in Ishida et al. (2022) for OASUCA except without the usage of cumulus parameterization and Wada et al. (2018) for NHM. The Regional Specialized Meteorological Center (RSMC) Tokyo best track data (<https://www.jma.go.jp/jma/eng/jma-center/rsmc-hp-pub-eg/besttrack.html>) is used to validate the results of numerical simulations.

3. Results

3.1 Simulated tracks and central pressures

Figure 1a shows the comparison of the RSMC-Tokyo best track with the simulation results. Although the results of track simulations in the NHM and CPL experiments show eastward biases compared with the best track, those in the ASUCA and OASUCA experiments are reasonable to the best track.

Figure 1b shows the timeseries of the RSMC-Tokyo best track central pressures along with the simulated ones. Unlike the result of track simulations in the ASUCA and OASUCA experiments, both models could not simulate the best-track decreasing rate of central pressure and the minimum central pressure.

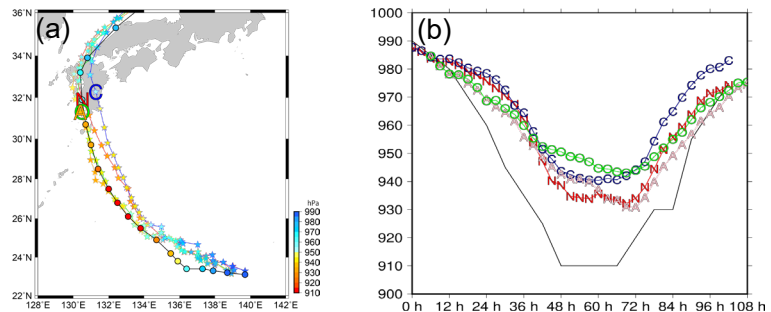


Figure 1 (a) RSMC-Tokyo best track positions (circles) every 6 hours with colors indicating the value of best-track central pressures with the positions (stars) simulated by the NHM (red), CPL (blue), ASUCA (orange) and OASUCA (green). The alphabets indicate the location of simulated typhoon at 00 UTC on 18 September in the NHM(N), CPL(C), ASUCA(A) and OASUCA(O) experiment. (b) Time series of RSMC-Tokyo best-track central pressures (black solid line) with the simulated ones. The abscissa in (b) is a relative time from 18UTC on 14 September.

The effect of ocean coupling on the simulated central pressure is represented by the difference of simulated central pressure between NHM and CPL and between ASUCA and OASUCA. The differences are relatively small in the early intensification phase and increase in the late intensification phase. The maxima of the differences were achieved in the mature phase. At 00UTC on 18 September, the difference in the simulated central pressures is still large in spite of the difference of the landfalling location between NHM and ASUCA (CPL and OASUCA).

3.2 Simulated sea surface temperatures

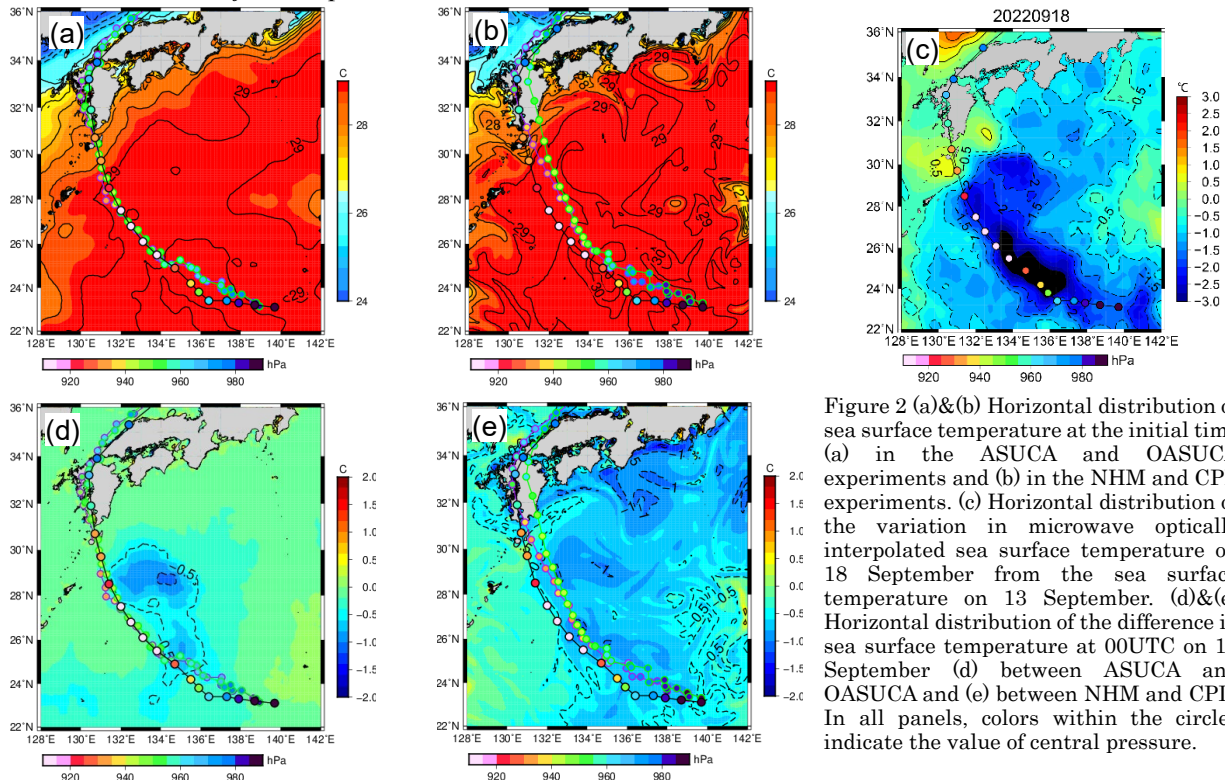


Figure 2 (a)&(b) Horizontal distribution of sea surface temperature at the initial time (a) in the ASUCA and OASUCA experiments and (b) in the NHM and CPL experiments. (c) Horizontal distribution of the variation in microwave optically interpolated sea surface temperature on 18 September from the sea surface temperature on 13 September. (d)&(e) Horizontal distribution of the difference in sea surface temperature at 00UTC on 18 September (d) between ASUCA and OASUCA and (e) between NHM and CPL. In all panels, colors within the circles indicate the value of central pressure.

At the initial time, the horizontal distribution of sea surface temperature used in the ASUCA and OASUCA experiments (Fig. 2a) is similar to that used in the NHM and CPL experiments (Fig. 2b) although a finer distribution is found in Fig. 2b. Microwave optically interpolated sea surface temperature data indicate that sea surface cooling was induced along the track after the passage of Nanmadol (Fig. 2c). The magnitude of the sea surface cooling exceeds 3°C . Sea surface cooling simulated in the OASUCA experiment is confined around the right-hand side of the track (Fig. 2d), while sea surface cooling in the CPL experiment (Fig. 2e) becomes similar to that analyzed by using the microwave optically interpolated sea surface temperature data (Fig. 2c). These differences in SST simulations between CPL and OASUCA do not, however, lead to the improvement of simulated track and central pressure. Rather, relatively small magnitude of simulated sea surface cooling may be attributed to relatively high minimum simulated central pressures.

3.3 Simulated rainfall at 00 UTC on 18 September

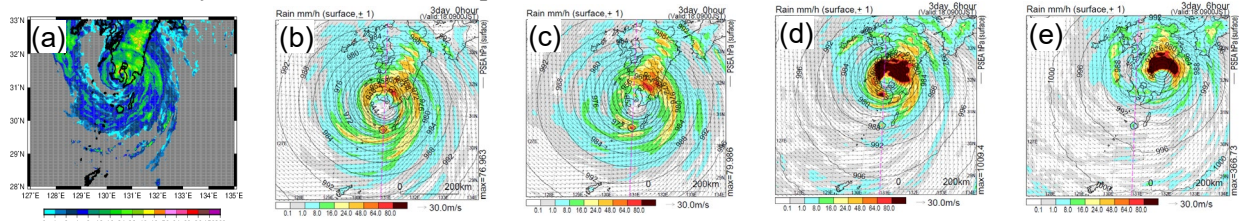


Figure 3 The 1-hour rainfall distribution (mm / hour) (a) analyzed every 10 minutes, simulated in the (b) ASUCA, (c) OASUCA, (d) NHM, and (e) CPL experiments at 00 UTC on 18 September.

Figure 3a shows the 1-hour rainfall distribution analyzed every 10 minutes. Shield-like heavy rainfall distribution is observed in Miyazaki Prefecture. All the simulation results show the occurrence of heavy rainfall in Miyazaki Prefecture, but the almost all the precipitation is simulated around the eyewall of simulated Nanmadol where the effect of ocean coupling on the precipitation amount is clearly found (Fig. 2b-2e). In other words, heavy precipitation in Miyazaki Prefecture induced by topography is not well improved by ocean coupling, which may be attributed to track errors particularly in the NHM and CPL experiments, and insufficient intensity simulations attributed to the structural change of the typhoon.

4. Future works

Numerical simulation experiments will be continued under the policy that improvements in the physical processes in the atmosphere model, rather than the effects of ocean coupling, are more important to more realistically reproduce both typhoon intensity and heavy precipitation associated with the typhoon.

References

- Ishida, J., K. Aranami, K. Kawano, K. Matsubayashi, Y. Kitamura, and C. Muroi, 2022: ASUCA: The JMA Operational Non-hydrostatic Model. *J. Meteor. Soc. Japan*, 100, 825-846, <https://doi.org/10.2151/jmsj.2022-043>.
- Wada, A., S. Kanada, and H. Yamada, 2018: Effect of air-sea environmental conditions and interfacial processes on extremely intense typhoon Haiyan (2013). *Journal of Geophysical Research: Atmospheres*, 123, 10379-10405, <https://doi.org/10.1029/2017JD028139>.

The impact of ocean coupling on the genesis of Typhoon Songda (2022) simulated by two atmosphere-ocean coupled models

Akiyoshi Wada*, Wataru Yanase, and Satoki Tsujino

Meteorological Research Institute, Tsukuba, Ibaraki, 305-0052, JAPAN

*awada@mri-jma.go.jp

1. Introduction

A tropical depression was formed around the edge of subtropical high northwest of the Mariana islands on 26 July in 2022. The tropical depression moved north northwestward along the edge of subtropical high and developed to a tropical storm Songda on 28 July. The Philippine Sea was covered with high sea-level pressure prior to the onset of a tropical depression with the sea surface temperature higher than 30°C. The area of high sea surface temperature expanded from the onset to the genesis of Songda. To investigate the impact of ocean coupling and high sea surface temperature extending east of Philippines on the genesis of Songda, we conducted numerical simulations using a nonhydrostatic atmosphere model, the non-hydrostatic numerical weather prediction model ASUCA (Ishida et al. 2022) coupled with an ocean model and the coupled atmosphere-wave-ocean model (Wada et al., 2018).

2. Experimental design

The atmosphere model ASUCA is an atmosphere model and this study uses the ASUCA coupled with a 1-dimensional ocean model (OASUCA). The coupled atmosphere-wave-ocean model (CPL) consists of a nonhydrostatic atmosphere model previously used as a numerical weather prediction model in the Japan Meteorological Agency (JMANHM), a mixed-layer ocean model and the third-generation ocean surface wave model. JMANHM is also used for the numerical simulation on the genesis of Songda.

Table 1 shows a list of numerical simulations. The computational domain is the same among the three simulations, NHM, CPL and OASUCA. The domain is 4500 km (zonal) x 2700 km (meridional) of which center location is 22.5°N, 130°E. The horizontal resolution is 3 km. The number of vertical layers is 96 for ASUCA (the top height is about 37 km) and 55 for NHM (the top height is about 27 km).

Table1 List of numerical simulations

Name	Model	Cumulus Parameterization (CP) & cloud physics
NHM	JMANHM	No CP & ice phase predicted
CPL	JMANHM coupled with a mixed layer ocean model and the third-generation ocean surface wave model (Wada et al. 2018)	No CP & ice phase predicted
OASUCA	ASUCA coupled with a 1-dimensional ocean model (Ishida et al. 2022)	No CP & ice phase predicted but the formation process of graupel is simplified.

All the simulations are started from 00UTC on 21 July in 2022. The integration period is 9 days (216 hours). An initial condition and 6-hourly boundary conditions for the atmosphere are created from the global objective atmospheric analysis data of the Japan Meteorological Agency (~20 km horizontal resolution). In addition, an initial condition for the ocean is created from the North Pacific version of the oceanic analysis data (~0. 1° horizontal resolution) merged with the Optimally Interpolated SST (OISST) daily product (0.25° horizontal resolution) obtained from the Remote Sensing Systems (<http://www.remss.com>) as of 20 July. In the OASUCA experiment, the World Ocean Atlas (WOA) 2018 (<https://www.ncei.noaa.gov/products/world-ocean-atlas>) and Merged satellite and in-situ data Global Daily Sea Surface Temperature (MGDSST) are used for creating oceanic initial conditions. Physical processes used in this study are standard as referred in Ishida et al. (2022) for OASUCA except without the usage of cumulus parameterization and Wada et al. (2018) for NHM. The Regional Specialized Meteorological Center (RSMC) Tokyo best track data (<https://www.jma.go.jp/jma/jma-eng/jma-center/rsmc-hp-pub-eg/besttrack.html>) is used to validate the results of numerical simulations.

3. Results

3.1 SST

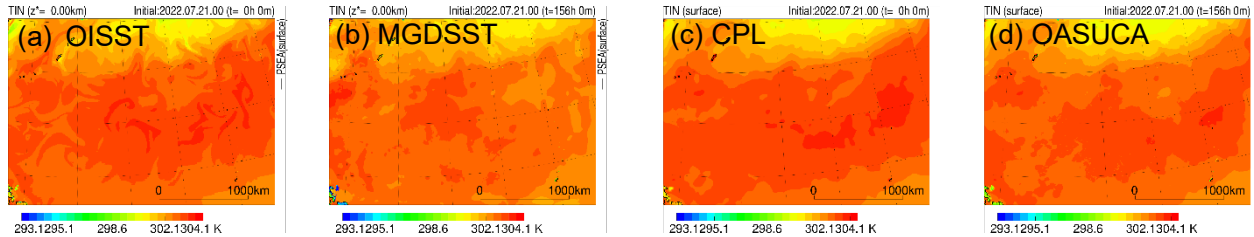


Figure 1 Horizontal distributions of sea surface temperature at 0 h obtained from (a) OISST and (b) MGDSST and at 156 h in the (c) CPL and (d) OASUCA experiments. The unit of sea surface temperature is K and the color range is from 293.15 K (20°C) to 304.15 K (31°C).

Figure 1 shows the horizontal distribution of sea surface temperature at 0 h used in the CPL (Fig. 1a) and OASUCA (Fig. 1b) experiments and at 156 h in the CPL (Fig. 1c) and OASUCA (Fig. 1d) experiments. All the numerical experiments successfully simulate an onset of tropical depression at the edge of subtropical high at 12 UTC on 27 July (Fig.2) although the OASUCA model simulates a tropical cyclone, which develops more rapidly

than the RSMC-Tokyo best track data . In this study, the simulated tropical depression is regarded as a precursor of Songda (2022). However, the area of high sea surface temperature east of the Philippines and east-west asymmetric pattern obtained from OISST at 12 UTC on 27 July (not shown) could not be reasonably simulated in the CPL (Fig. 1c) and OASUCA (Fig. 1d) experiments. Simulated sea surface temperature in the CPL experiment (Fig. 1c) becomes realistically low east of the computational domain compared to that in the OASUCA experiment (Fig. 1d).

3.2 Wind speeds at the lowermost level

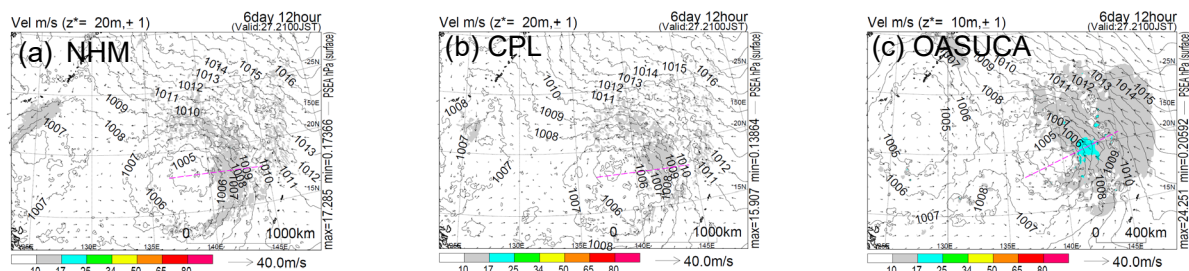


Figure 2 Horizontal distributions of wind speeds at an altitude of 20 meters at 156 h in the (a) NHM and (b) CPL experiments, and those at an altitude of 10 meters at 156 h in the (c) OASUCA experiment. A dashed magenta line in each panel shows a cross-section line in Fig.3.

Figure 2 shows the horizontal distributions of wind speeds near the surface. All the simulations show relatively high wind speed exceeding 10 m s^{-1} northeast to east of a tropical depression. The OASUCA (Fig. 2c) simulates wind speeds exceeding 10 m s^{-1} at a higher altitude than the NHM (Fig. 2a) and CPL (Fig. 2b) around the edge of subtropical high. This indicates that the impact of ocean coupling on wind speeds near the surface is relatively small compared with that of the difference of the atmosphere model between OASUCA and NHM.

3.3 Vertical wind structure across the center of tropical depression

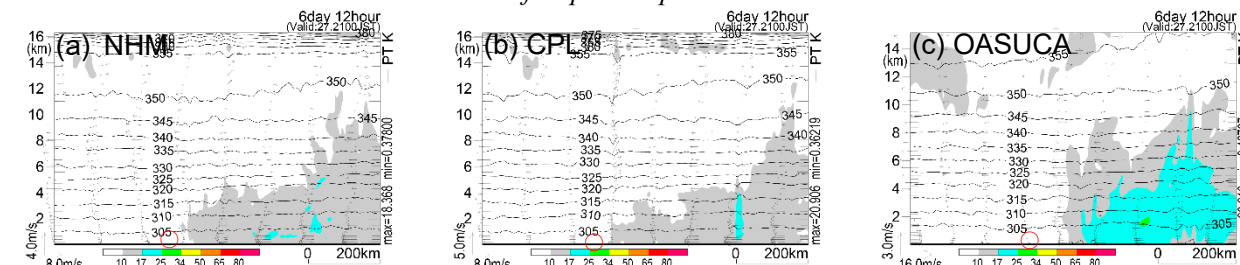


Figure 3 Vertical sections of simulated wind speeds with simulated potential temperatures at 156 h in the (a) NHM, (b) CPL, and (c) OASUCA experiments. The location of cross section is shown in each panel of Figure 2. Red circles correspond to the location of convergence near the surface.

Figure 3 shows the cross section of simulated wind speeds with simulated potential temperature across the center of a simulated tropical depression in the NHM (Fig. 3a) and CPL (Fig. 3b) experiments and across the center of a tropical cyclone in the OASUCA experiment (Fig. 3c). The magnitude of simulated wind speeds around the edge of subtropical high is greater in the OASUCA experiment (Fig. 3c) than in the NHM (Fig. 3a) and CPL (Fig. 3b) experiments. The locations of the tropical depressions and the tropical cyclone correspond to the area of relatively weak convergence. Those are not affected by the impact of ocean coupling and the difference in the models used in this study.

4. Concluding remarks

We conducted numerical simulations on an onset of Songda in 2022 using JMANHM, CPL and OASUCA models. From the results of numerical simulations, we obtain the following results.

1. The impact of sea surface temperature on an onset of a tropical depression is relatively small.
2. Wind speeds at an altitude of 10 meters simulated by the OASUCA model are higher than those at an altitude of 20 meters simulated by the NHM and CPL models.
3. The locations of the convergence of surface winds are not affected by the impact of ocean coupling as well as the difference between the models, which may be regarded as characteristics of the formation of a tropical depression or a tropical cyclone.

It should be noted that the OASUCA model tends to overdevelop the tropical depression to a tropical cyclone compared to the RSMC-Tokyo best track analysis although the simulated track is more reasonable to the best track than the CPL model. The relation of high winds around the edge of subtropical high and simulated track will be one of the subjects in the future.

References

- Ishida, J., K. Aranami, K.Kawano, K. Matsubayashi, Y. Kitamura, and C. Muroi, 2022: ASUCA: The JMA Operational Non-hydrostatic Model. J. Meteor. Soc. Japan, 100, 825-846, <https://doi.org/10.2151/jmsj.2022-043>.
- Wada, A., S. Kanada, and H. Yamada, 2018 : Effect of air–sea environmental conditions and interfacial processes on extremely intense typhoon Haiyan (2013). Journal of Geophysical Research: Atmospheres, 123, 10379-10405, <https://doi.org/10.1029/2017JD028139>.